50th AIAA Aerospace Sciences Meeting including the New Horizons Forum and Aerospace Exposition
09 - 12 January 2012, Nashville, Tennessee
AIAA 2012-0324

On the Unsteady Thrust Measurement for Pulse Detonation Engines

Dibesh D. Joshi[1] and Frank K. Lu[2]
University of Texas at Arlington, Arlington, TX, 76019

A pulse detonation engine simulator operating at 5 and 20 Hz was used to study unsteady thrust characteristics. The natural vibration frequencies, the effective mass of the simulator and the steady thrust were first determined. The system dynamics of the simulator, deconvolved in the frequency domain, was studied. The impulse transfer function was used to reconstruct the thrust response and acceleration compensation was applied to get the thrust solely due to the pulsating jet. The thrust response of the system due to exit of the pulsed jet could be reconstructed well. The acceleration compensation technique enabled the actual thrust to be recovered from reconstructed signal. Pulse-to-pulse interference was not observed for the frequencies tested.

I. Introduction

THE unsteady thrust measurement for pulse detonation engines (PDEs) is likely to be affected by the inertial load due to acceleration.[1] Thus, conventional thrust measurement techniques need to be extended to account for the cyclic acceleration of the structure. A method which requires identification of the system's dynamic parameters has been well-established in thrust measurements in shock tunnels.[8-17] A similar situation occurs for a single pulse of a PDE. Additionally, in the present situation, unlike an impulse facility, a pulse train forms and the effect of interference between the pulses is not well understood. Parameter identification and acceleration compensation techniques were implemented to extract the correct thrust values from load cell measurements.

For developing the unsteady thrust measurement technique, a PDE simulator as shown in Fig.1 is used. The simulator utilized pulses of pressurized air driven into it near the closed end of the tube at the right of the figure, which generated thrust upon exit from the open end to the left. The thrust and the pressure were measured. A correction method, accounting the system's acceleration, was used to recover the actual thrust that is solely due to the unsteady flow. The approach first required determination of the impulse transfer function of the system based on the input, which consisted of a single pulse of pressurized air, to the system and the output measured by load cell. Once the transfer function was established, a deconvolution procedure was carried out to reconstruct the thrust. Furthermore, the effective mass of the system which contributes for cyclic acceleration was determined. From the reconstructed thrust, the cyclic load, which is the product of the effective mass and measured acceleration, was subtracted to obtain the actual thrust.[7] The method was then applied at pulsed frequencies of 5 and 20 Hz.

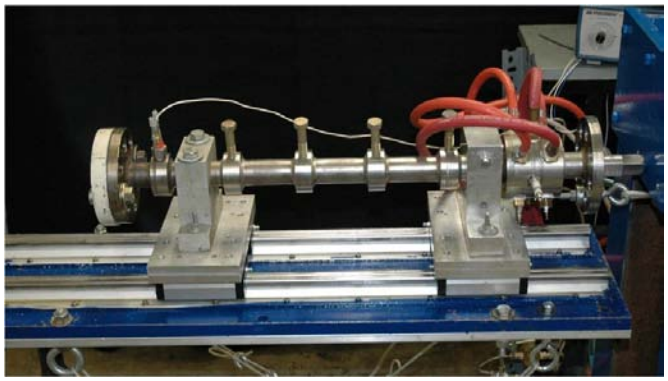

Figure 1. Experimental setup for PDE simulator.

II. Method

A. Approach

[1]Graduate Research Assistant, Mechanical and Aerospace Engineering Department, AIAA Student Member.
[2]Professor and Director, Aerodynamics Research Center, Mechanical and Aerospace Engineering Department, Box 19018, AIAA Associate Fellow.

The method first requires the determination of the transfer function of the system $g(t)$ based on the input pressure $p(t)$ and the output $f(t)$. This procedure is applied to a single pulse as described in the following paragraph. For a linear system, one can write the relationship between the input, the output and the transfer function by the convolution integral[3]

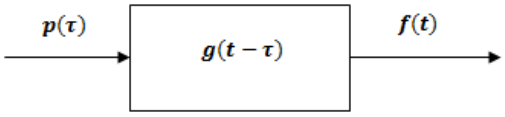

Figure 2. Block diagram for system identification approach.

$$f(t) = \int_0^t p(\tau) g(t-\tau) d\tau \tag{1}$$

If the input to the system is known, a deconvolution of Eq. (1) yields the transfer function. Once the transfer function is known, then any arbitrary output can be determined from a measurement of the input and vice versa.

An impulse of pressurized air can be used as the input,

$$p(t) = \delta(t) \tag{2}$$

$$f(t) = \int_0^t \delta(\tau) g(t-\tau)\, d\tau \tag{3}$$

Applying a Fourier transform to Eq. (3) yields the impulse transfer function in the frequency domain

$$G(s) = \frac{F(s)}{P(s)} \tag{4a}$$

where $P(s)$ and $F(s)$ are the Fourier transforms of the input and output respectively. Hence, from the measurement of the output and the input, an impulse transfer function can be determined experimentally. With this established transfer function and a subsequent measured input, the output $F1(s)$ is given by

$$F1(s) = G(s)\, P1(s) \tag{4b}$$

where $G(s)$ is the previously established impulse transfer function and $P1(s)$ is the Fourier transform of the measured input. Once the impulse transfer function is established, it can then be used subsequently to deconvolve the dynamic response of the entire structure from the actual thrust. However, the structure also undergoes a distinct acceleration. Since the pulses are repetitive, the acceleration is also repetitive.

Deconvolving the dynamic response from the thrust does not necessarily compensate for these repetitive accelerations as the cyclic load from the acceleration is inherently fused to the thrust signals. A separate procedure is needed for the acceleration compensation. Assuming a linear relation between acceleration and corresponding cyclic load, the added cyclic load can be compensated using

$$F_{corr} = F_{deconv} - m_{eff}.a_{filt} \tag{5}$$

where, F_{deconv} is the deconvolved thrust signal using the impulse transfer function, m_{eff} is the effective mass of the structure that is actively oscillating and contributing to the cyclic load, a_{filt} is the filtered acceleration signal which is obtained after truncating the measured acceleration signals to retain the acceleration information (i.e., removing noise), and F_{corr} is the actual thrust generated by the PDE.

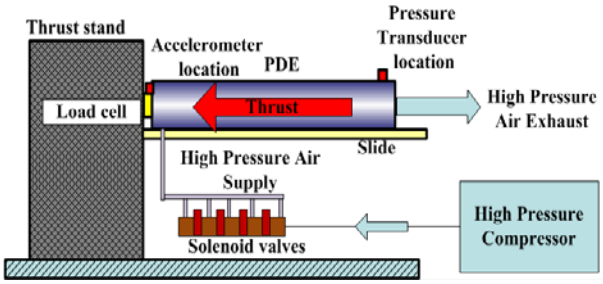

Figure 3. Schematic of experimental setup.

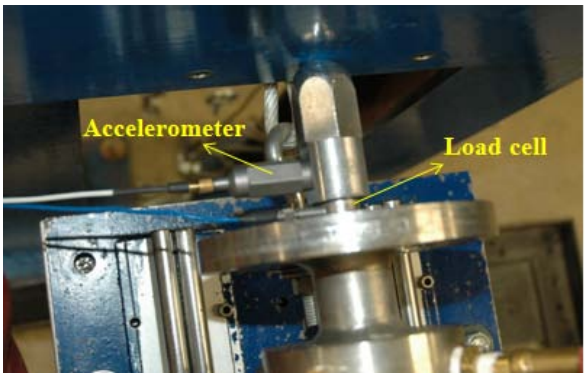

Figure 4. Mounting of accelerometer and load cell.

B. Hardware

An actual pulse detonation engine is a complicated piece of hardware. Therefore, for this study, a pulse detonation engine simulator was

built. The PDE simulator, made of stainless steel, is shown in Fig. 1 and a schematic of the entire setup is shown in Fig. 3. The simulator consisted of a pipe that was 26 in. long and that had an inner diameter of 1 in. The pipe was mounted on a slide to allow it to move. As shown in Fig. 1, the simulator had flanges at both ends and it was supported at two locations. From one side, the simulator was butted against a load cell (PCB Model 201B02) and supported by a thrust stand. The load cell measured the thrust generated when the pulsed pressurized air exited the PDE simulator. The load cell was preloaded to 100 lbf, which was required for the dynamic force measurements as per manufacturer's specification.

A compression-type multi-axial accelerometer (PCB Model 302B03) was used to measure the acceleration of the simulator. The accelerometer was mounted right next to the load cell using a stud mount on a steel load concentrator which was supported by the thrust stand as shown in Fig. 4. The simulator had inlet ports for pressurized air to be fed into the tube at different frequencies. The pressure of the leaving air was measured at the exit end of the simulator by a pressure transducer (PCB Model 111A24). The flow was pulsed by solenoid valves (Dayton Model 1A575) with orifice diameter of 1/8 in. Since the orifice diameter of the solenoid valves are small, five of them were used to supply adequate air to the simulator for generating measurable thrust. The exits of the solenoid valves were connected to the simulator by air hoses with ¼ in. inner diameter. The valves were normally closed and required a 120 VAC coil (Dayton Model 3A440) for activation. The operation of the solenoid valves was controlled by a function generator (BK-Precision Model 4010A). The function generator sent square wave signals to the solenoid valves at set frequencies, thus controlling the operating frequency of the solenoid valves. However, the high power electrical circuitry of five solenoids valves could not be directly controlled by the small electronic circuitry of the function generator.[18] Hence a digital control system was used to interface the set of five solenoids valves with the function generator. Since the function generator produces an analog TTL output signal, a simple circuit using economical components was built to make the analog signal imitate a digital outcome. The interface circuit consisted of Darlington transistors to drive low power 24 VDC SPDT relay which in turn drove the solenoid coils. The function generator voltage output was passed to the transistor which activated the low power relay thus controlling the solenoid valves. The transistor was incorporated in the circuit since the power output of the function generator was already low.

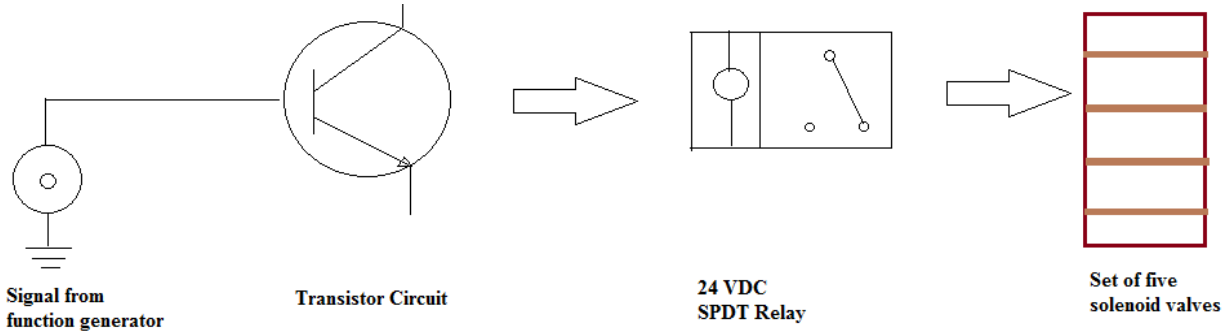

Figure 5. Solenoid valves control system schematic.

III. Results and Discussion

A. Natural Free Vibration Test

An impact hammer (PCB Model 086C01) was used to impulsively excite the dynamics of the PDE simulator with the output registered by the accelerometer. Since the relaxation time of the excited system is greater than the duration of the impulsive input, the resulting system output was regarded as the natural or the free vibration response. The time domain input, which is the impulsive excitation from the hammer, and the resulting output response of the system were examined in the frequency domain via an FFT.

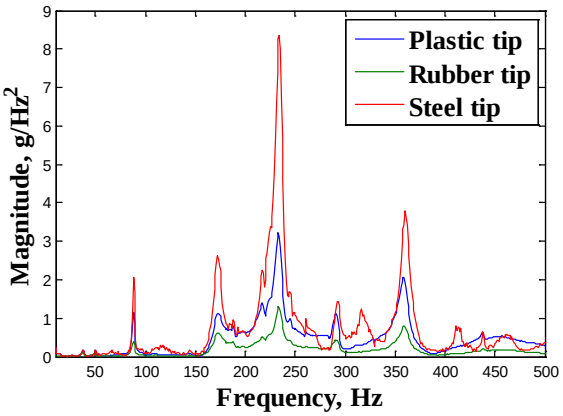

Figure 6. Frequency response of the system to impulsive excitation.

Figure 6 shows the frequency response of the PDE simulator when struck by the hammer with a steel, a plastic or a rubber tip. Efforts were made to apply a similar impulsive force in every case. Figure 6 shows the frequency range of 5–500 Hz with distinct peaks at 88, 172, 234, 293 and 360 Hz. These frequencies were the natural or free vibration frequencies of the system. Application of a forcing frequency at the above mentioned frequencies were avoided to prevent system resonance as would be most likely in a PDE. In the simulation experiments to be discussed later, the pulsed air was driven at 5 or 20 Hz. Thus, the recorded load cell response is not fraught by dynamic response of the system brought about by the resonance response of the system.

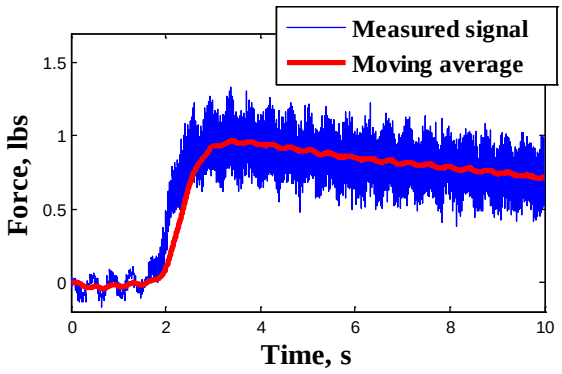

Figure 7. Steady thrust due to steady pressure input.

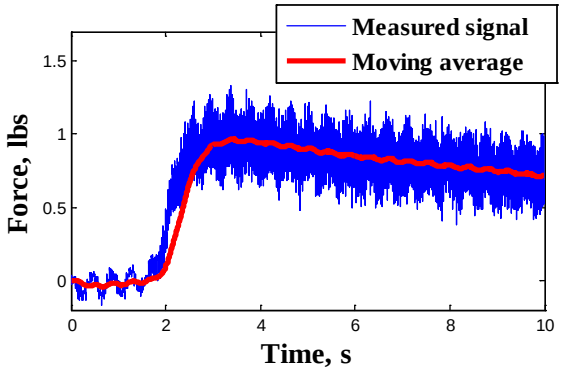

Figure 8. Steady pressurized air driven into the system.

B. Steady Operation Test

Although the PDE operates in a pulsed manner and the thrust generated is unsteady, it is still useful to obtain the steady thrust. The steady thrust was measured by exhausting a steady jet at inlet pressures of 190, 275 and 360 psia. Both generated thrust and pressure at the exit of the simulator were measured at 200,000 samples per second. Figures 7 and 8 show the thrust and the pressure measured at the exit for the case when the high pressure source was pumped to 360 psia. A moving average of the measured signal was taken to smoothen out the curves and improve the signal-to-noise ratio. Several pressure values and the corresponding thrust values from the averaged curves were used to create a thrust vs. pressure chart for steady operation as shown in Fig. 9. This procedure is valid considering that the pulsed operation occurs at a frequency of at least 5 Hz and integration window of 1 second is sufficient for steady operation case. For the steady operation case, it is observed that there is linear relation between pressure and thrust.

C. Determination of Effective Mass

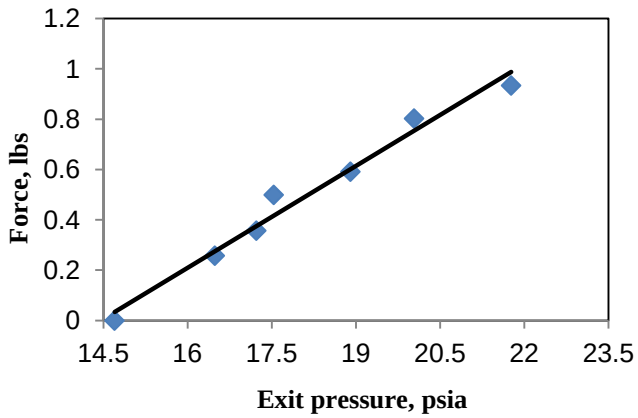

Figure 9. Relation between force and pressure for the steady operation case.

When the PDE simulator was operated, the whole structure underwent cyclic acceleration. Even though the system motion was extremely small due to preloading, the structure underwent oscillations when the pulsed air exited the system. The extent and the duration of oscillations depended on the thrust from the pulsations. Equation (5) introduces a term m_{eff} which represents the oscillating mass of the simulator[7]. The effective mass depends on the force applied to the simulator. Thus, a relation between the applied force and m_{eff} was established to choose a proper value of the latter for the acceleration compensation technique.

After striking the system impulsively by an impact hammer, the generated impulsive force was measured by the load cell and the resulting oscillations were measured by the accelerometer. Both the impulsive force and oscillations of the system were sampled at 200,000 samples per second. The impulsive forces were applied in such a way that they were within the measurable range of the load cell.

The root mean squared value of measured impulsive force and oscillation were calculated. The rms was only taken for that portion of the signal where the magnitude of oscillations was prominent. For example, Fig. 10 shows the rms interval of the force and acceleration taken where the magnitude of the oscillations measured by the accelerometer was prominent. With a calculated rms values of impulsive force and resulting oscillations, $m_{effective}$ was determined by

$$m_{eff} = \frac{F_{impulse}}{a_{measured}} \qquad (6)$$

Figure 11 shows the variation of effective mass for a range of applied impulsive forces. From Fig. 11, it can be concluded that as the magnitude of impulsive force increases the effective mass decreases. This property holds true since a higher impulsive force excites the system more providing higher magnitude of oscillations. Substituting the rms of measured values in Eqn. (6) yields a smaller effective mass, as summarized in Fig. 11. Therefore, Fig. 11 was used to estimate the effective mass of the system for a particular value of applied force.

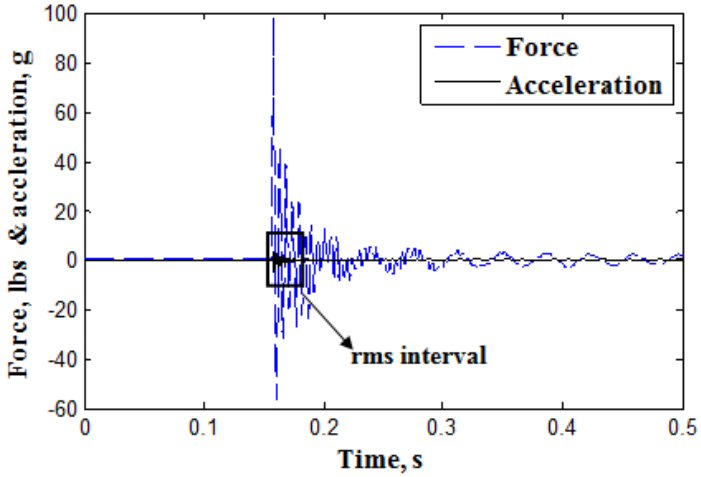

Figure 10. Measured force and acceleration due to impulsive force of 98 lbs.

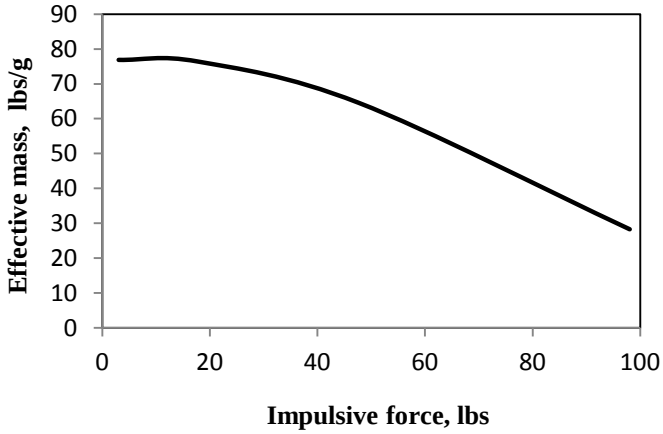

Figure 11. Effective mass calculated for a range of impulsive force applied.

D. Signal Reconstruction for pulsed cases

Signals were acquired at a rate of 800,000 samples per second. Sampling at high frequency helped to increase the temporal resolution. However, high sampling rates also adds high-frequency noise to the signals from which the thrust needed to be deconvolved. As mentioned in the approach, first an impulse transfer function was established. This was done in the frequency domain by dividing the measured output shown in Fig. 12 by the input, a single pressure pulse, shown in Fig. 13. Once the transfer function was established, deconvolution was carried out by reconstructing the thrust using the established transfer function and the measured input via Eq. (4b). Figures 14 and 15 show the magnitude and phase spectra of the impulse transfer function. In both spectra, the frequency spectrum is normalized by the number of samples. Figures 16 and 17 show the input pulsed pressurized airflow at 5 and 20 Hz respectively. Figures 18 and 19 show the reconstructed thrust signal by a red line for 5 and 20 Hz respectively. In both cases, the reconstructed thrust was greater than the measured thrust. The reconstructed thrust signals were noisier than the measured signals; this may be because of digital artifacts of the FFT. A further refinement to the reconstructed signal should be implemented, which is an area for future work. Both measured and reconstructed thrust signals shown in Figs. 18 and 19 do not exhibit any prominent interference between consecutive thrust pulses. The response generated due to the exit of a pressure pulse has enough time to die out before the occurrence of another one. It is possible that interference between adjacent pressure pulses can significantly affect the thrust when the frequency is higher.

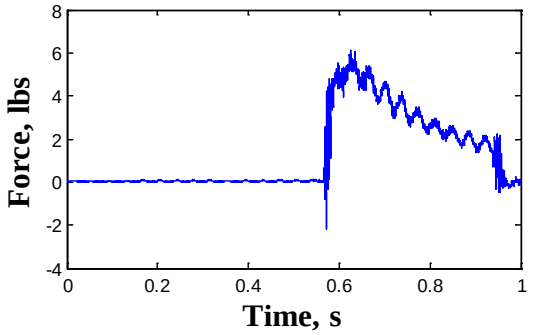

Figure 12. Response of the system due to single pressure pulse.

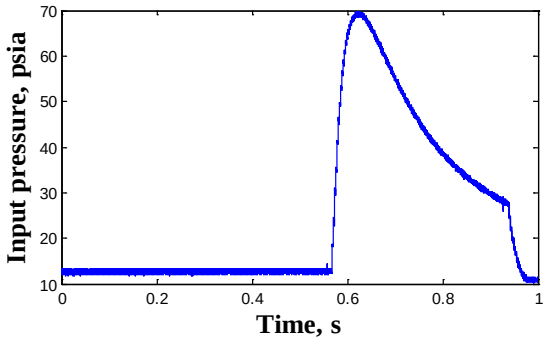

Figure 13. Single pressure pulse driven into the system.

E. Acceleration Compensation

Acceleration compensation was applied to get the actual thrust from the reconstructed signals since the cyclic load due to acceleration is inherently fused to the thrust signal. The cyclic load can be successfully compensated from the thrust signal using Eqs. (5) and (6). The process first required the determination of the effective mass of the system contributing to the cyclic load. This can be done through a comparative study using Fig. 11. For the 5 Hz case, it can be observed from Fig. 18 that the applied force to the system due to the exit of the pulsed pressurized air is close to 5 lbs. With this applied force known, the effective mass of the system for this case was determined to be 76 lbs/g using Fig. 11. Similarly for the 20 Hz case, the effective mass was determined to be 77 lbs/g.

For the proper application of Eq. (5), the acceleration for each case must be known. The acceleration for each run was measured and examples are shown in Figs. 20 and 21. A band-pass Butterworth filter was applied to retain acceleration information. The low and high cutoff for the filter was selected to be 185 and 250 Hz respectively. Example filtered acceleration signals are also shown in Figs. 20 and 21 for 5 Hz and 20 Hz case respectively. In both these cases, the filtered acceleration signals oscillated around the zero line and showed a very low magnitude because the thrust was low. The product of the effective mass and the filtered acceleration was subtracted from the reconstructed thrust to get the actual thrust. The acceleration compensated thrust is shown in Figs. 22 and 23.

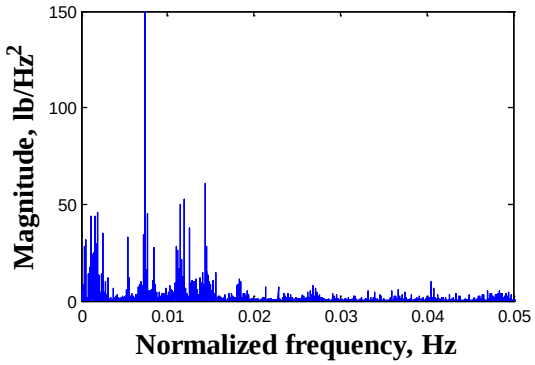

Figure 14. Magnitude spectrum of experimental transfer function.

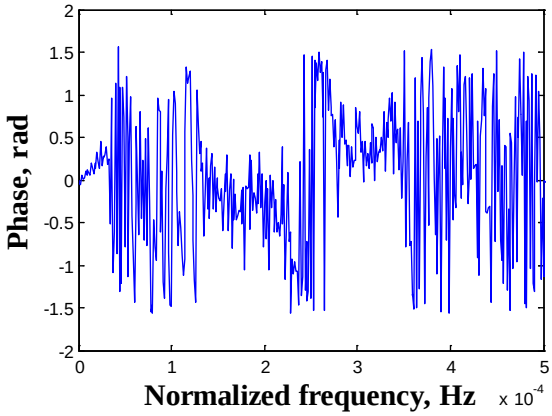

Figure 15. Phase spectrum of experimental transfer function.

IV. Conclusions

A PDE simulator was used to study the unsteady thrust characteristics. Experiments were first performed to determine the natural vibration frequencies and study the simulator's steady operation. After this, it was concluded that operating the simulator at 5 or 20 Hz does not lead the system to resonance. A technique was developed to determine the effective mass of the system contributing to the cyclic loads. Moreover, a general approach was developed to obtain the actual thrust. The approach first required the impulse transfer function of the system to be determined so as to reconstruct the thrust signal from the measured input. From the reconstructed thrust, the cyclic load was subtracted to get the actual thrust. The cyclic load for the simulator is the product of effective mass and measured acceleration during each run.

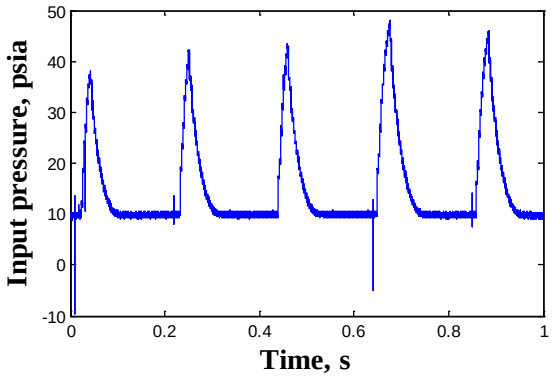

Figure 16. Measured 5Hz pulsed input.

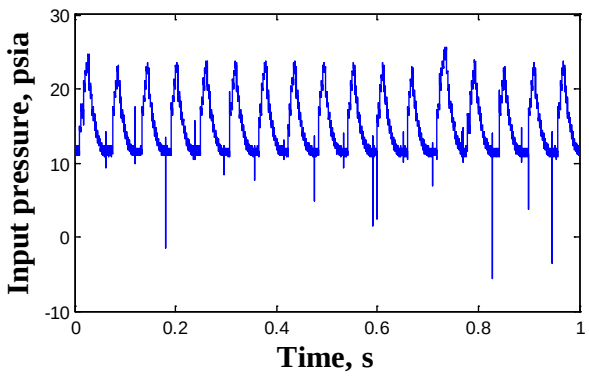

Figure 17. Measured 20 Hz pulsed input.

The method was tested for 5 and 20 Hz pulsed inputs. It was concluded that the thrust signals could be reconstructed well from the input using the impulse transfer function. Compensating for cyclic load yielded the actual thrust. However, the measured acceleration was very low hence there was no significant difference between the reconstructed and compensated thrust. Also, no prominent interference between the thrust pulses was observed upon reconstruction.

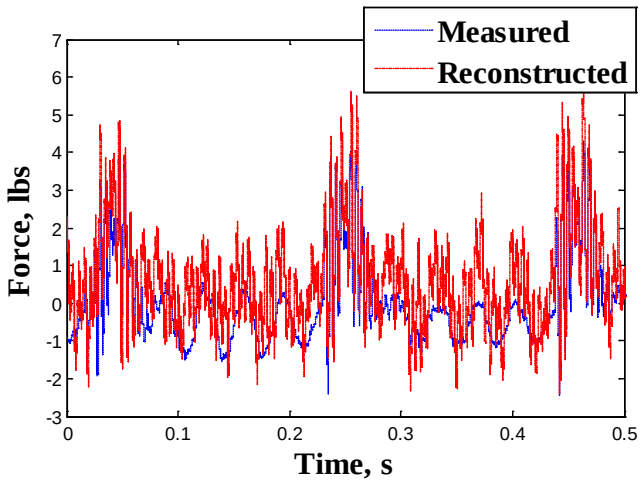

Figure 18. Measured and reconstructed thrust for 5 Hz case.

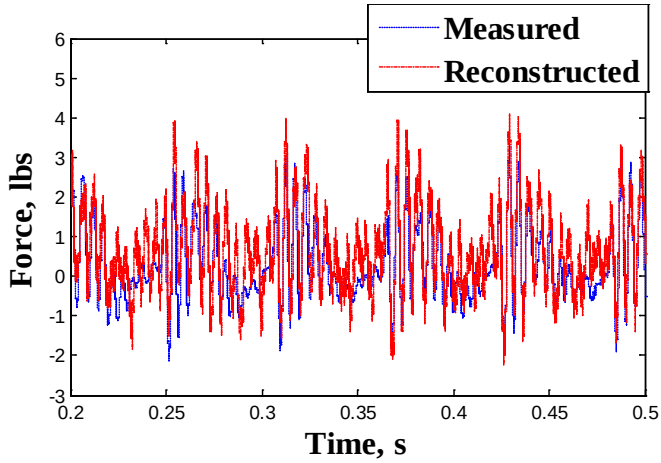

Figure 19. Measured and reconstructed thrust for 20 Hz case.

Acknowledgements

The authors gratefully acknowledge the help from Professors David Mee of the University of Queensland and Professor Herbert Olivier of RWTH in providing detailed information on dynamic calibration techniques.

References

[1]Lu, F.K., Awasthi, M. and Joshi, D.D., "Influence of Unsteadiness on Thrust Measurements of Pulse Detonation Engines," AIAA Paper 2010-1214, 2010.

[2]Bernstein, L. "Force Measurement in Short-Duration Hypersonic Facilities," AGARDograph AGARD-AG-214, 1975.

[3]Naumann, K.W., Ende, H. and Mathieu, G., "Technique for Aerodynamic Force Measurement within Milliseconds in Shock Tunnel," *Shock Waves*, Vol. 1, No. 3, 1991, pp. 223–232.

[4]Sanderson, S.R. and Simmons, J.M., "Drag Balance for Hypervelocity Impulse Facilities," *AIAA Journal*, Vol. 29, No. 12, 1991, pp. 2185–2191.

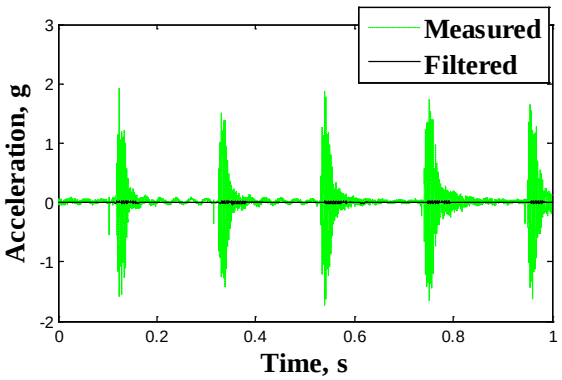

Figure 20. Measured and filtered acceleration For 5 Hz case.

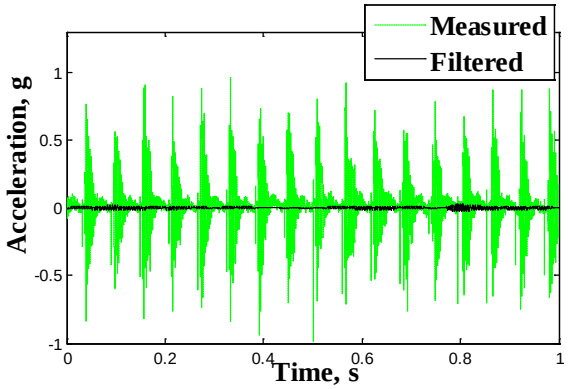

Figure 21. Measured and filtered acceleration for 20 Hz case.

[5]Daniel, W.J.T. and Mee, D.J., "Finite Element Modelling of a Three-Component Force Balance for Hypersonic Flows," *Computers & Structures*, Vol. 54, No. 1, 1995, pp. 35-48.

[6]Smith, A.L. and Mee, D.J., "Drag Measurements in a Hypervelocity Expansion Tube," *Shock Waves*, Vol. 6, No. 3, 1996, pp. 161–166.

[7]Storkmann, V. Olivier, H. and Grönig H., "Force Measurements in Hypersonic Impulse Facilities," *AIAA Journal*, Vol. 36, No. 3, 1998, pp. 342–348.

[8]Sahoo, N., Mahapatra, D.R., Jagadeesh, G., Gopalakrishnan, S. and Reddy, K.P.J., "An accelerometer balance system for measurement of aerodynamic force coefficients over blunt bodies in a hypersonic shock tunnel," *Measurement Science and Technology*, Vol. 14, No. 3, 2003, pp. 260–272.

[9]Mee, D.J., "Dynamic Calibration of Force Balances for Impulse Hypersonic Facilities," *Shock Waves*, Vol. 12, No. 6, 2004. pp. 443–455.

[10]Joarder, R. and Jagadeesh, G., "A New Free Floating Accelerometer Balance System for Force Measurements in Shock Tunnels," *Shock Waves*, Vol. 13, No. 5, 2004. pp. 409–412.

[11]Sahoo, N., Suryavamshi, K., Reddy, K.P.J. and Mee, D.J., "Dynamic force balances for short-duration hypersonic testing facilities," *Experiments in Fluids*, Vol. 38, No. 5, 2005, pp. 606–614.

[12]Tanno, H., Kodera, M., Komuro, T., Sato, K., Takahasi, M. and Itoh, K., "Aerodynamic Force Measurement on a Large-Scale Model in a Short Duration Test Facility," *Review of Scientific Instruments*, Vol. 76, 035107, 2005.

[13]Robinson, M.J., Mee, D.J. and Paull, A., "Scramjet Lift, Thrust and Pitching-Moment Characteristics Measured in a Shock Tunnel," *Journal of Propulsion and Power*, Vol. 22, No. 1, 2006, pp. 85–95.

[14]Sahoo, N., Mahapatra, D.R., Jagadeesh, G., Gopalakrishnan, S. and Reddy, K.P.J., "Design and Analysis of a Flat Accelerometer-Based Force Balance System for Shock Tunnel Testing," *Measurement*, Vol. 40, No. 1, 2007, pp. 93–106.

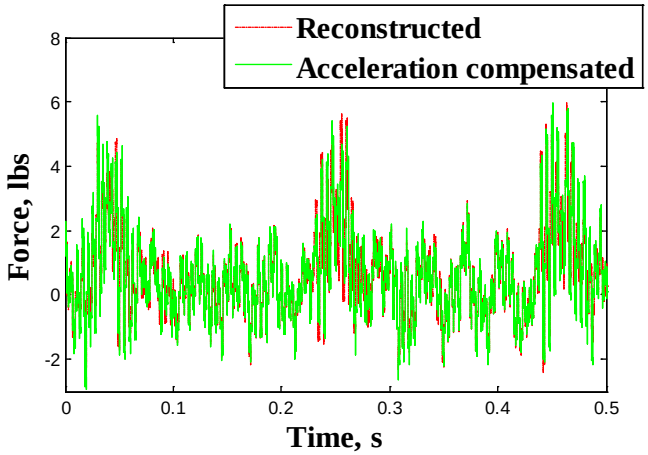

Figure 22. Reconstructed and acceleration compensated thrust for 5 Hz case.

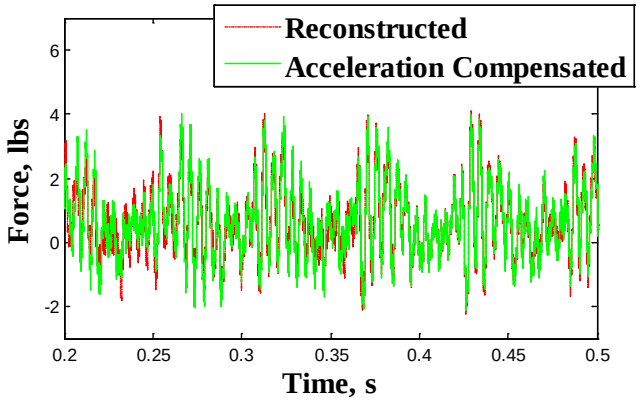

Figure 23. Reconstructed and acceleration compensated thrust for 20 Hz case.

[15]Abdel-Jawad, M.M., Mee, D.J. and Morgan, R.G., "New Calibration Technique for Multiple-Component Stress Wave Force Balances," *Review of Scientific Instruments*, Vol. 78, 2007, Article No. 065101.

[16] Ketsdever, A.D., D'Souza, D.C. and Lee, R.H., "Thrust Stand Micromass Balance for the Direct Measurement of Specific Impulse," *Journal of Propulsion and Power*, Vol. 24, No. 6, 2008, pp. 1376–1381.

[17] Satheesh, K. and Jagadeesh, G., "Analysis of an Internally Mountable Accelerometer Balance System for use with Non-Isotropic Models in Shock Tunnels, *Measurement*, Vol. 42, No. 6, 2009, pp. 856–862.
[18] Braun, E. M., Lu, F.K., Panicker, P.K., Mitchell, R. R., Wilson,D. R. and Dutton, J. C., " Supersonic Wind Tunnel Control Using LabView,"*46th Aerospace Sciences Meeting and Exhibit,* AIAA Paper 2008-852, January 7-10, 2008, Reno, Nevada.